REPORT DOCUMENTATION PAGE

AFRL-SR-AR-TR-03-

0472

PLEASE DO NOT RETURN YOUR FORM TO THE ABOVE ADDRESS.

1. REPORT DATE *(DD-MM-YYYY)*	2. REPORT TYPE	3. DATES COVERED *(From - To)*
30092003	Final Report	September 1, 02 - September 30, 03

4. TITLE AND SUBTITLE
Exploitation of Omnidirectional Reflectivity

5a. CONTRACT NUMBER

5b. GRANT NUMBER
F49620-02-C-0076

5c. PROGRAM ELEMENT NUMBER

6. AUTHOR(S)
Dr. Tri Van
Dr. Dennis Nyquist
Dr. Leo Kempel
Dr. Gang Bao

5d. PROJECT NUMBER

5e. TASK NUMBER

5f. WORK UNIT NUMBER

7. PERFORMING ORGANIZATION NAME(S) AND ADDRESS(ES)
Mission Research Corporation
735 State Street
Santa Barbara, CA 93101

8. PERFORMING ORGANIZATION REPORT NUMBER

9. SPONSORING/MONITORING AGENCY NAME(S) AND ADDRESS(ES)
Department of the Air Force
Air Force Office of Scientific Research
4015 Wilson Blvd.
Arlington, VA 22203-1954

10. SPONSOR/MONITOR'S ACRONYM(S)

11. SPONSOR/MONITOR'S REPORT NUMBER(S)

12. DISTRIBUTION/AVAILABILITY STATEMENT

Approved for public release, distribution unlimited.

20031121 008

13. SUPPLEMENTARY NOTES
DODAAD CODE: 1G992
AFOSR Program Manager: Dr. Arje Nachman

14. ABSTRACT

In this final report, we have summarized the progress made during the period of September 1. 2002- September 30, 2003. We derive the integral equations for (electric fields propagating in a fiber of arbitrary cross section and arbitrary refractive index. Mathematical analysis of conventional optical fibers is rich and widely available in literature, for example [3, 9, 11] and references therein. It helps the advancement of optical fiber industry in understanding and designing fibers for data transport and telecommunications. In Contrary, to our best knowledge, there is little of rigorous mathematical study of Bragg fibers due to the fabrication difficulty. Recently, the publications of A dielectric omnidirectional reflector [4], An all-dielectric coaxial wave guide [8], and External reflection from omnidirectional dielectric mirror fibers [7] in Science report successful fabrications of omnidirectional reflectors and multi-layered fibers for optical wavelengths. These articles create a new interest in studying low-loss Bragg fibers at microwave and millimeter wavelengths for radar applications. From previous examples in Section 4, multi-layered fibers of radii between 7 mm and 19 mm concentrate wave propagation within their air core for wavelengths in the microwave range.

15. SUBJECT TERMS

16. SECURITY CLASSIFICATION OF:			17. LIMITATION OF ABSTRACT	18. NUMBER OF PAGES	19a. NAME OF RESPONSIBLE PERSON
a. REPORT	b. ABSTRACT	c. THIS PAGE			Dr. Tri Van
					19b. TELEPHONE NUMBER *(Include area code)*

Exploitation of Omnidirectional Reflectivity

Contract number: F49620-02-C-0076

Topic: AF02T015

Final Report

September 1, 2002 – September 30, 2003

Tri Van* Dennis Nyquist† Leo Kempel‡ Gang Bao§

Abstract

This is the final report for Phase I of the above STTR contract with AFOSR during the period September 1, 2002 - September 30, 2003. It is based on Status Reports 1, 2, and 3. We summarize the development of integral equations and their numerical implementations in solving wave propagation in a cylindrical fiber with concentric dielectric layers. These multilayered fibers are also called Bragg fibers [12, 13, 15]. From preliminary computational results, we find that an air-core multilayered fiber can effectively guide wave in its air core when its total radius is a quarter of the operating wavelength.

1 Introduction

An omnidirectional reflector which reflects electromagnetic radiation from all incoming angles and over a broad range of frequencies but exhibits virtually no absorption losses has been fabricated for the 20,000 GHz – 30,000 GHz frequency range [4]. Recently, an omnidirectional dielectric mirror fiber which is an omnidirectional reflector of cylindrical shape with the diameter of 200 μm, has been developed by Yoel Fink and his colleagues [7]. These omnidirectional dielectric mirrors can be used in applications requiring optimal confinement or reflection of light at all angles, such as optical cavities or hollow waveguide. It is of great interest to the Air Force if omnidirectional reflectors and fibers which operate in the lower frequency range can be fabricated.

*Mission Research Corporation, 3975 Research Blvd., Dayton, OH, 45430. Email: tvan@mrcday.com

†Department of Electrical and Computer Engineering, Michigan State University, East Lansing, MI, 48824. Email: nyquist@egr.msu.edu

‡Department of Electrical and Computer Engineering, Michigan State University, East Lansing, MI, 48824. Email: kempel@egr.msu.edu

§Department of Mathematics, Michigan State University, East Lansing, MI, 48824. Email: bao@math.msu.edu

Microwave (MW, 1 GHz – 18 GHz) and millimeter wave (MMW, 18 GHz – 100 GHz) frequencies are particularly desirable (see Fig. 1) in radar technology.

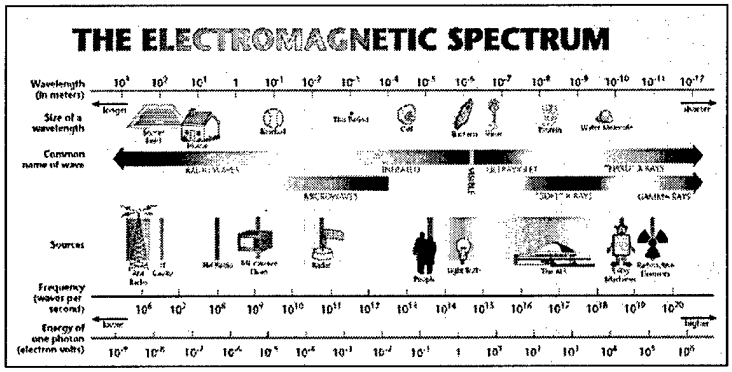

Figure 1: Electromagnetic spectrum

Based on experience and published data, it is likely that high performance omnidirectional reflectors for lower frequencies (MW and MMW) will be too thick to be practical. Hence, at lower frequencies there is a need for higher contrast ratio layer structures, to enhance the reflection coefficient at each interface to maintain a reasonable overall thickness. However, the use of higher contrast systems will lead to a reduction in angle coverage. Therefore, to determine the low frequency region where an omnidirectional reflector and a low-loss dielectric fiber are viable and candidate materials for achieving required performance, it is important to perform analytical and numerical study of the wave propagation in the planar and cylindrical dielectric layered structures.

In our preliminary study of Bragg fibers, it is possible to concentrate electromagnetic wave in an air core Bragg fiber whose radius is comparable to wavelengths in the microwave region. Further investigation and analysis are necessary to reach a more definite conclusion.

Omnidirectional reflectivity, the ability to reflect waves at arbitrary angle of incidence, is possible in multilayered dielectric media whose band diagrams consist of spectral regions where no light transmission exists in the media, which are called band gaps. For planar multilayered stacks, transfer matrix method has been used in computing their band structures and reflectance spectra (see, e.g., [1, 2, 5, 14]).

Unlike conventional fibers, which guide light through *total internal reflection*, Bragg fibers achieve light confinement through *Bragg reflection* [13]. Bragg fibers uses a one-dimensional periodicity of concentric rings that exhibit omnidirectional reflection in the planar limit. In other words, in the limit of large radius, the circular Bragg fiber approaches a planar Bragg stack, whose band diagrams consist of band gaps. Therefore, it is necessary to have Bragg fiber modes to fall inside the TM and/or TE band gaps of the corresponding Bragg stack.

Wave propagation in a Bragg fiber can be analyzed by a transfer matrix approach and the minimization of radiation loss as in [15], or by numerically solving Maxwell's equations using finite difference method in both frequency and time domains. Recently, asymptotic matrix theory of Bragg fibers is developed in [13]. Yeh's transfer matrix-minimization method is complicated for guided modes that are not TM nor TE. In order to use finite difference methods, one needs to construct fictitious boundary conditions such as perfectly matched layers (PML) or absorbing boundary conditions (ABC). They can be also time-consuming. The asymptotic matrix analysis

fails if the fiber core becomes too small and it is difficult to estimate the accuracy of the asymptotic results. Operating wavelengths in these articles are in the optical region of the electromagnetic spectrum.

The rest of the report is arranged as follows. In Section 2, we present the electric field integral equation which describes wave propagation in a cylindrical waveguide of arbitrary shape. In Section 3, Nÿstrom method is employed to discretize integral equations. The approach is simple but very efficient. In order to determine propagating modes, non-linear eigenvalue problem needs to be solved. Newton's method and Ridder's algorithm are implemented to find solutions of the eigenvalue problem. In Section 4, numerical examples are given to illustrate the validity of the integral equation formulation and numerical techniques. Finally, the report is concluded in Section 5. Here, we also draw attention to mathematical issues that require detailed and rigorous investigation.

2 Integral equations

In this section, we briefly present the EFIE to describe the surface-wave propagation in a dielectric cylindrical waveguide. First, the general 3-D EFIE for a waveguide with a graded-index core of arbitrary cross section shape is introduced. The 3-D EFIE is then reduced to a 2-D EFIE when the index profile n is axially-uniform, that is, $n(x,y,z) = n(\rho,\theta)$. Finally, for a graded-index circular fiber with the radially-graded index core, i.e., $n(x,y,z) = n(r)$, we further reduce the 2-D EFIE to a system of 1-D integral equations. We are especially interested in *natural surface wave modes* which are nontrivial modal solutions to the homogeneous EFIE when the incident field $\boldsymbol{E}^i = 0$.

In integrated dielectric waveguide system with a dielectric waveguide whose refractive index profile is described by $n(x,y,z)$, lying on the planar interface $\{y = 0\}$ between a substrate having index n_s and a cladding overlay of index n_c (e.g., air with $n_c = n_0$), the fundamental electric field integral equation can be expressed as

$$\boldsymbol{E}(\boldsymbol{r}) - (k_c^2 + \nabla\nabla\cdot)\int_V \frac{\delta n^2(\boldsymbol{r}')}{n_c^2}\bar{\bar{G}}(\boldsymbol{r},\boldsymbol{r}')\cdot\boldsymbol{E}(\boldsymbol{r}')dV' = \boldsymbol{E}^{inc}(\boldsymbol{r}),$$

where $\delta n^2(\boldsymbol{r}) = n^2(\boldsymbol{r}) - n_c^2$, V is the volume where $\delta n^2 \neq 0$, $k_c = \omega\sqrt{\mu_0\varepsilon_c} = \omega\sqrt{\mu_0\varepsilon_0}\sqrt{\varepsilon_c/\varepsilon_0} = k_0 n_c$, and $\bar{\bar{G}}(\boldsymbol{r},\boldsymbol{r}')$ is the 3-D Hertzian potential Green's dyadic defined as

$$\bar{\bar{G}}(\boldsymbol{r},\boldsymbol{r}') = \bar{\bar{G}}^p(\boldsymbol{r},\boldsymbol{r}') + \bar{\bar{G}}^r(\boldsymbol{r},\boldsymbol{r}'),$$

with $\bar{\bar{G}}^p$ is the principal Green's dyadic for primary wave of Hertzian potential excited by polarization and $\bar{\bar{G}}^r$ is the reflected Green's dyadic for reflected wave of Hertzian potential excited at the substrate-overlay interface. Note that if $n_s = n_c$ (the substrate is removed), $\bar{\bar{G}}^r = 0$. The principal Green's dyadic is defined as

$$\bar{\bar{G}}^p(\boldsymbol{r},\boldsymbol{r}') = \frac{e^{ik_c|\boldsymbol{r}-\boldsymbol{r}'|}}{4\pi|\boldsymbol{r}-\boldsymbol{r}'|}\bar{\bar{I}}.$$

The formula of $\bar{\bar{G}}^r$ is omitted for brevity. In the rest of the report, we are interested in natural surface-wave modes which are the solutions to the homogeneous EFIE when $\boldsymbol{E}^{inc} = 0$ and for $n_s = n_c$.

2.1 EFIE for axially-uniform waveguides

Consider the z-uniform waveguide whose refractive index profile is z-independent, that is, $n(\boldsymbol{r}) = n(\boldsymbol{\rho})$, where $\boldsymbol{\rho} = x\hat{x} + y\hat{y}$. Consequently, the electric field $\boldsymbol{E}$ can be written as

$$\boldsymbol{E}(\boldsymbol{r}) = \boldsymbol{e}(\boldsymbol{\rho})e^{-i\beta z}, \quad \boldsymbol{\rho} = x\hat{x} + y\hat{y},$$

where β is the propagating constant which is an unknown eigenvalue parameter. The homogenous EFIE becomes

$$\boldsymbol{e}(\boldsymbol{\rho}) - (k_c^2 + \nabla\nabla\cdot)\int_\Omega dS' \frac{\delta n^2(\boldsymbol{\rho}')}{n_c^2}\bar{\bar{g}}(\boldsymbol{\rho},\boldsymbol{\rho}')\cdot\boldsymbol{e}(\boldsymbol{\rho}') = 0, \tag{1}$$

where Ω is the cross section of the waveguide and

$$\bar{\bar{g}}(\boldsymbol{\rho},\boldsymbol{\rho}') = g(\boldsymbol{\rho},\boldsymbol{\rho}')\bar{\bar{I}} = \frac{K_0(\gamma_c|\boldsymbol{\rho}-\boldsymbol{\rho}'|)}{2\pi}\bar{\bar{I}},$$

with

$$\gamma_c = \sqrt{\beta^2 - k_c^2}. \tag{2}$$

By using divergence theorem, one can show that transverse components of (1) are independent and hence yield a *unique* description of the surface-wave modes. Therefore, it is sufficient to consider the following equation for the transverse components $\boldsymbol{e}_t = e_x\hat{x} + e_y\hat{y}$ of $\boldsymbol{e}$:

$$\begin{aligned}\boldsymbol{e}_t(\boldsymbol{\rho}) - \nabla_t\left(-\oint_\Gamma \frac{\delta n^2(\boldsymbol{\rho}')}{n_c^2}\hat{n}'\cdot\boldsymbol{e}_t(\boldsymbol{\rho}')g(\boldsymbol{\rho},\boldsymbol{\rho}')dl' + \int_\Omega \frac{\nabla_t' n^2(\boldsymbol{\rho}')\cdot\boldsymbol{e}_t(\boldsymbol{\rho}')}{n^2(\boldsymbol{\rho})}g(\boldsymbol{\rho},\boldsymbol{\rho}')dS'\right) \\ +k_0^2\int_\Omega \delta n^2(\boldsymbol{\rho}')\boldsymbol{e}_t(\boldsymbol{\rho}')g(\boldsymbol{\rho},\boldsymbol{\rho}')dS' = 0, \quad \forall\boldsymbol{\rho}\in\Omega,\end{aligned} \tag{3}$$

where $\Gamma = \partial\Omega$, $\hat{n}'$ is the outward normal of the boundary Γ, and $\nabla_t = \frac{\partial}{\partial x}\hat{x} + \frac{\partial}{\partial y}\hat{y}$.

2.2 EFIE for axially-uniform circular waveguides

Assume that the index profile of the waveguide only varies radially, that is, $n(\boldsymbol{\rho}) = n(r)$. In (3), we note that $\hat{n}'\cdot\boldsymbol{e}_t = \hat{r}'\cdot\boldsymbol{e}_t = e_r$, thus, the homogeneous EFIE in polar coordinates can be expressed as

$$\begin{aligned}\boldsymbol{e}_t(r,\phi) - \nabla_t\left(-\oint_\Gamma \frac{\delta n^2(r')}{n_c^2}e_r(r',\phi')\frac{K_0(\gamma_c|\boldsymbol{\rho}-\boldsymbol{\rho}'|)}{2\pi}dl' + \int_\Omega \frac{dn^2(r')}{dr'}\frac{e_r(r',\phi')}{n^2(r')}\frac{K_0(\gamma_c|\boldsymbol{\rho}-\boldsymbol{\rho}'|)}{2\pi}dS'\right) \\ -k_0^2\int_\Omega \delta n^2(r')\boldsymbol{e}_t(r',\phi')\frac{K_0(\gamma_c|\boldsymbol{\rho}-\boldsymbol{\rho}'|)}{2\pi}dS' = 0.\end{aligned}$$

We can decompose the above vector EFIE into two coupled EFIE's for the scalar fields e_r and e_ϕ as

$$\begin{aligned}e_r(r,\phi) - \frac{\partial}{\partial r}\left[-\oint_\Gamma \frac{\delta n^2(a)}{n_c^2}e_r(a,\phi')\frac{K_0(\gamma_c|\boldsymbol{\rho}-\boldsymbol{\rho}'|)}{2\pi}dl' + \int_\Omega \frac{dn^2(r')}{dr'}\frac{e_r(r',\phi')}{n^2(r')}\frac{K_0(\gamma_c|\boldsymbol{\rho}-\boldsymbol{\rho}'|)}{2\pi}dS'\right] \\ -k_0^2\int_\Omega \delta n^2(r')[e_r(r',\phi')\cos(\phi-\phi') + e_\phi(r',\phi')\sin(\phi-\phi')]\frac{K_0(\gamma_c|\boldsymbol{\rho}-\boldsymbol{\rho}'|)}{2\pi}dS' = 0,\end{aligned}$$

$$e_\phi(r,\phi) - \frac{1}{r}\frac{\partial}{\partial\phi}\left[-\oint_\Gamma \frac{\delta n^2(a)}{n_c^2} e_r(a,\phi')\frac{K_0(\gamma_c|\boldsymbol{\rho}-\boldsymbol{\rho}'|)}{2\pi}dl' + \int_\Omega \frac{dn^2(r')}{dr'}\frac{e_r(r',\phi')}{n^2(r')}\frac{K_0(\gamma_c|\boldsymbol{\rho}-\boldsymbol{\rho}'|)}{2\pi}dS'\right]$$
$$-k_0^2\int_\Omega \delta n^2(r')[-e_r(r',\phi')\sin(\phi-\phi') + e_\phi(r',\phi')\cos(\phi-\phi')]\frac{K_0(\gamma_c|\boldsymbol{\rho}-\boldsymbol{\rho}'|)}{2\pi}dS' = 0$$

We can write the unknown scalar field components are represented by Fourier series with radially-dependent coefficients in the angular variable ϕ as

$$e_r(r,\phi) = \sum_{m=-\infty}^{\infty} A_{r,m}(r)e^{im\phi}, \qquad e_\phi(r,\phi) = \sum_{m=-\infty}^{\infty} iA_{\phi,m}(r)e^{im\phi}. \tag{4}$$

Substituting (4) into the integral equations for e_r and e_ϕ yields the integral equations for the radial coefficients $A_{r,m}(r)$ and $A_{\phi,m}(r)$: for $0 < r < a$ where a is the radius of the circular waveguide,

$$\begin{array}{l} A_{r,m}(r) - \int_0^a A_{r,m}(r')\left[-\dfrac{\delta(r'-a)\delta n^2(r')}{n_c^2} + \dfrac{1}{n^2(r')}\dfrac{dn^2(r')}{dr'}\right]\dfrac{\partial W_{0,\gamma_m}(r,r')}{\partial r}r'dr' \\ -k_0^2\int_0^a \delta n^2(r')[A_{r,m}(r')W_{c,\gamma_m}(r,r') - A_{\phi,m}(r')W_{s,\gamma_m}(r,r')r'dr' = 0, \end{array} \tag{5}$$

and

$$\begin{array}{l} A_{\phi,m}(r) - \dfrac{n}{r}\int_0^a A_{r,n}(r')\left[-\dfrac{\delta(r'-a)\delta n^2(r')}{n_c^2} + \dfrac{1}{n^2(r')}\dfrac{dn^2(r')}{dr'}\right]W_{0,\gamma_m}(r,r')r'dr' \\ -k_0^2\int_0^a \delta n^2(r')[-A_{r,n}(r')W_{s,\gamma_m}(r,r') + A_{\phi,m}(r')W_{c,\gamma_m}(r,r')]r'dr' = 0, \end{array} \tag{6}$$

where γ_m is defined by (2) and the kernels W_{0,γ_m}, W_{c,γ_m} and W_{s,γ_m} are defined as

$$\begin{aligned} W_{0,\gamma_m}(r,r') &= \frac{1}{2\pi}\int_{-\pi}^{\pi} e^{im\psi}K_0(\gamma_m\sqrt{r^2+r'^2-2rr'\cos\psi})d\psi \\ &= \begin{cases} K_n(\gamma_m r)I_n(\gamma_m r') & \text{if } r' < r, \\ I_m(\gamma_m r)K_m(\gamma_m r') & \text{if } r' > r, \end{cases} \end{aligned}$$

$$\begin{aligned} W_{c,\gamma_m}(r,r') &= \frac{1}{2\pi}\int_{-\pi}^{\pi} e^{im\psi}\cos\psi K_0(\gamma_m\sqrt{r^2+r'^2-2rr'\cos\psi})d\psi \\ &= \frac{1}{2}\begin{cases} K_{m+1}(\gamma_m r)I_{m+1}(\gamma_m r') + K_{m-1}(\gamma_m r)I_{m-1}(\gamma_m r') & \text{if } r' < r, \\ I_{m+1}(\gamma_m r)K_{m+1}(\gamma_m r') + I_{m-1}(\gamma_m r)K_{m-1}(\gamma_m r') & \text{if } r' > r, \end{cases} \end{aligned}$$

and

$$\begin{aligned} W_{s,\gamma_m}(r,r') &= \frac{1}{2\pi}\int_{-\pi}^{\pi} e^{im\psi}\sin\psi K_0(\gamma_m\sqrt{r^2+r'^2-2rr'\cos\psi})d\psi \\ &= \frac{1}{2}\begin{cases} K_{m+1}(\gamma_m r)I_{m+1}(\gamma_m r') - K_{m-1}(\gamma_m r)I_{m-1}(\gamma_m r') & \text{if } r' < r, \\ I_{m+1}(\gamma_m r)K_{m+1}(\gamma_m r') - I_{m-1}(\gamma_m r)K_{m-1}(\gamma_m r') & \text{if } r' > r. \end{cases} \end{aligned}$$

3 Computational method

Integral equations (5) and (6) are discretized by Nÿstrom method [10]. Since kernels W_0, W_c, and W_s are in closed forms, the implementation of the method is simple.

3.1 Nÿstrom's method

Nÿstrom method is used to discretize (5) and (6). For brevity, the interval $(0, a)$ is divided into segments of length $\Delta r = a/N$ where N is the number of subintervals. Denote $r_i = i * h$, $i = 1, 2, \ldots, N$ and $r_0 = \epsilon$ for some $0 < \epsilon \ll 1$. First, the integrals in (5) and (6) are approximated by the composite trapezoidal rule. Hence, we get

$$A_{r,m}(r) - \sum_{j=0}^{N} w_j A_{r,m}(r_j) \left[-\frac{\delta(r_j - a)\Delta n^2(r_j)}{n_c^2} + \frac{1}{n^2(r_j)} \frac{dn^2(r_j)}{dr'} \right] \frac{\partial W_{0,\gamma_m}(r, r_j)}{\partial r} r_j \Delta r$$
$$-k_0^2 \sum_{j=0}^{N} w_j \Delta n^2(r_j) [A_{r,m}(r_j) W_{c,\gamma_m}(r, r_j) - A_{\phi,m}(r_j) W_{s,\gamma_m}(r, r_j) r_j \Delta r = 0,$$

and

$$A_{\phi,m}(r) - \frac{m}{r} \sum_{j=0}^{N} A_{r,m}(r_j) \left[-\frac{\delta(r_j - a)\Delta n^2(r_j)}{n_c^2} + \frac{1}{n^2(r_j)} \frac{dn^2(r_j)}{dr'} \right] W_{0,\gamma_m}(r, r_j) r_j \Delta r$$
$$-k_0^2 \sum_{j=0}^{N} \Delta n^2(r_j) [-A_{r,m}(r_j) W_{s,\gamma_m}(r, r_j) + A_{\phi,m}(r_j) W_{c,\gamma_m}(r, r_j)] r_j \Delta r = 0,$$

where $w_0 = w_N = 0.5$ and $w_j = 1$ for $j \neq 0, N$. Now, setting $r = r_i$ for $i = 0, 1, \ldots, N$, we get the non-linear eigenvalue problem

$$[I - M(\gamma_m)]\, A = 0, \quad m = 0, 1, 2, \ldots, \tag{7}$$

where $M(\gamma_m)$ is a square matrix of size $2(N+1) \times 2(N+1)$ and $A = [A_r \; A_\phi]^T$ is the column vector consisting of the unknowns $A_{r,m}(r_i)$ and $A_{\phi,m}(r_i)$. For each given m, we denote

$$\Gamma_m = \left\{ 0 < \gamma_m^l \leq k_0 \sqrt{n_{max}^2 - n_{cl}^2},\; l = 1, 2, \ldots \right\}$$

as the set of allowable solutions where $n_{max} = \max_{0<r<a} n(r)$. The problem (7) has solution if and only if

$$\det [I - M(\gamma_m)] = 0. \tag{8}$$

3.2 Root finding problem

The solutions of the determinant equation (8) can be found by either Newton-Raphson's method or Ridder's method. These methods are both implemented for this report. Let γ_n go from 0 to $\Gamma = k_0 \sqrt{\max n^2 - n_c^2}$. When both the real part and imaginary of the determinant change their sign in one step, we use the Newton-Raphson method or Ridder's method to search for the zero of the determinant in this interval. In the Newton-Raphson, the derivative of M can be expressed in a closed form and we have

$$\gamma_m^{(k+1)} = \gamma_m^{(k)} - \frac{1}{trace\left\{ [M(\gamma_m^{(k)})]^{-1} \dfrac{dM}{d\gamma_m}(\gamma_m^{(k)}) \right\}}, \quad k = 0, 1, 2, \ldots, \tag{9}$$

where *trace* is the trace of a matrix, and $\gamma_m^{(0)}$ is the midpoint of the interval in consideration. In (9) we need to compute the matrix

$$B(\gamma_m^{(k)}) = [M(\gamma_m^{(k)})]^{-1} \frac{dM}{d\gamma_m}(\gamma_m^{(k)}).$$

One can efficiently do this by solving

$$M(\gamma_m^{(k)})B(\gamma_m^{(k)}) = \frac{dM}{d\gamma_m}(\gamma_m^{(k)}). \tag{10}$$

To simplify the notations, we denote the above problem as $MB = D$. We use the following procedure [6]

Compute $PM = LU$.
for $k = 1 : m$
    Solve $Ly = PD_k$
    Solve $Ub_k = y$
end

where D_k is the kth column of D.

4 Numerical experiments

In this section, we present several numerical examples which illustrate the convergence and accuracy of the integral equation formulation. We first consider the step-index fiber since its exact solutions are available. It can be seen from the computed data that the integral formulation is very accurate with even the simplest discretization method (trapezoidal rule). In the following numerical examples, the parameters are unitless. We choose operating wavelengths in terms of the radius of a fiber. In each example, we plot the absolute value of the normalized field solution of E_r and of E_r as a function of r and as a function of (r, ϕ). All results are computed with Matlab.

4.1 Step-index fiber

Consider a step-index fiber with

$$n_0 = 1.6,\ n_c = 1.0,\ a = 1,\ \lambda = 2a. \tag{11}$$

In this case, we can obtain the transcendental equation

$$\left(\frac{J_m'(u)}{uJ_m(u)} + \frac{K_m'(w)}{wK_m(w)}\right)\left(\frac{n_0^2}{n_c^2}\frac{J_m'(u)}{uJ_m(u)} + \frac{K_m'(w)}{wK_m(w)}\right) = m^2\left(\frac{1}{u^2} + \frac{1}{w^2}\right)\left(\frac{n_c^2}{n_0^2}\frac{1}{u^2} + \frac{1}{w^2}\right), \tag{12}$$

where

$$u = a\sqrt{k_0^2 n_0^2 - \beta^2}, \quad w = a\sqrt{\beta^2 - k_0^2 n_c^2}, \quad k_0 = \frac{2\pi}{\lambda}.$$

In Tables 1, 2, and 3, we compare the solutions γ_m to (8) with the "exact" solutions to the transcendental equation (12). In each table, N denotes the number subintervals in $[0, a]$. If $m = 0$, we obtain γ_{TE} and γ_{TM}. In Figures 2 and 3, we plot the electric field distributions and their intensity distributions, respectively. It is evident from the tables and figures that solutions to integral equations are very accurate. The convergence rate can be improved when more sophisticated quadratures are applied.

N	γ_{TM}	γ_{TE}
32	2.18506665	2.55757995
64	2.18337629	2.55601272
128	2.18295441	2.55562134
512	2.18282263	2.55549906
1024	2.18281604	2.55549294
exact	2.18281384	2.55549091

Table 1: Exact solutions and integral equation solutions for the TE and TM modes (mode number $m = 0$).

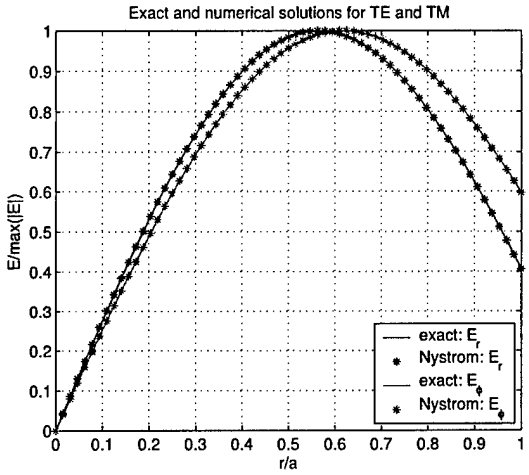

Figure 2: Exact and Nÿstrom solutions for TE (E_r) and TM (E_ϕ) cases. The number of subintervals used in the Nÿstrom method is $N = 128$.

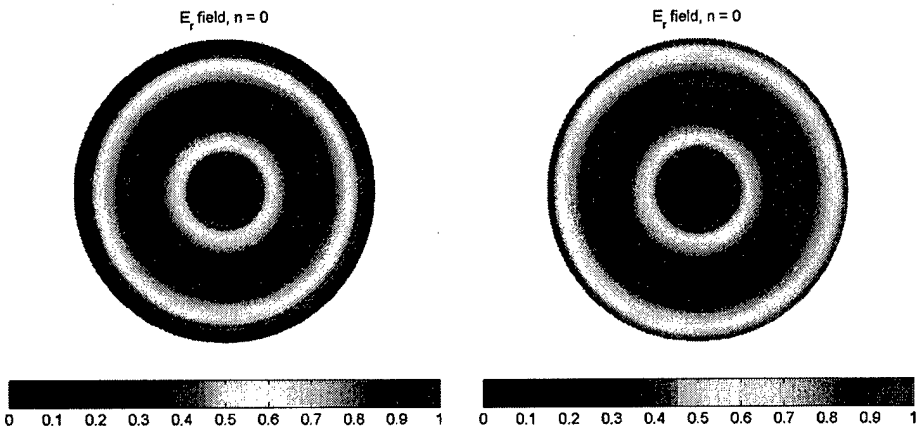

Figure 3: Intensity: $|E_r|^2$ and $|E_\phi|^2$.

N	$\gamma_{1,2}$	$\gamma_{1,1}$
32	0.57962508	3.34572448
64	0.57603586	3.34467642
128	0.57513626	3.34441567
512	0.57491122	3.34435058
1024	0.57485495	3.34433431
exact	0.57483619	3.34432888

Table 2: Exact and integral equation γ for the hybrid modes (mode number $m = 1$).

N	$\gamma_{2,1}$
32	2.20503141
64	2.20316831
128	2.20270322
512	2.20258699
1024	2.20255793
exact	2.20254824

Table 3: Exact and integral equation γ for the hybrid modes (mode number $m = 2$).

4.2 Multilayered fiber

Consider the following multilayered dielectric fiber immersed in air with the air core and 12 layers of dielectric pairs, which can schematically be written as $n_{\text{air}}^{\text{core}}(n_H n_L)_{12} n_{\text{air}}^{\text{ext}}$. The fiber parameters are

$$\begin{aligned} n_{\text{air}} = 1,\ n_H = 4.6,\ n_L = 1.5, \\ d_{\text{core}} = 1,\ d_H = 0.25,\ d_L = 0.75. \end{aligned} \tag{13}$$

Here, $n_{\text{air}}^{\text{core}} = 1$ denotes the air-core region and $n_{\text{air}}^{\text{ext}} = 1$ denotes the air region exterior to the fiber. The fiber radius is $d_{\max} = 1 + 12(.25 + .75) = 13$. The operating wavelength is $\lambda = 15.5$. Hence, if the unit of the radius is in millimeters (mm), the corresponding wavelength is 15.5 mm which is in the microwave region. In Figures 4 and 5, we plot the solutions E_r and E_ϕ and their intensity distributions for $m = 1$ and $\gamma = 1.03184$. Here we use the following grid sizes

$$h_{\text{core}} = d_{\text{core}}/10, \quad h_H = d_H/15, \quad h_L = d_L/20.$$

We note that most of the field is concentrated in the air core and the first layer ($0 < r < 2$). The ability to guide waves in the air core is of importance since non-linear effects and propagation loss are reduced significantly.

4.3 Quarter-wavelength fibers

We now consider quarter-wavelength multilayered fibers, that is, their radii are a quarter of the operating wavelength. This has no relation to the quarter-wave dielectric mirrors or stacks [5]. The thickness of the high-index layer and the low-index layer can be identical or different. In the following examples, we solve for propagating wave whose mode number is $m = 1$. It can be seen from the plots of intensity distributions that most of propagating field is concentrated in

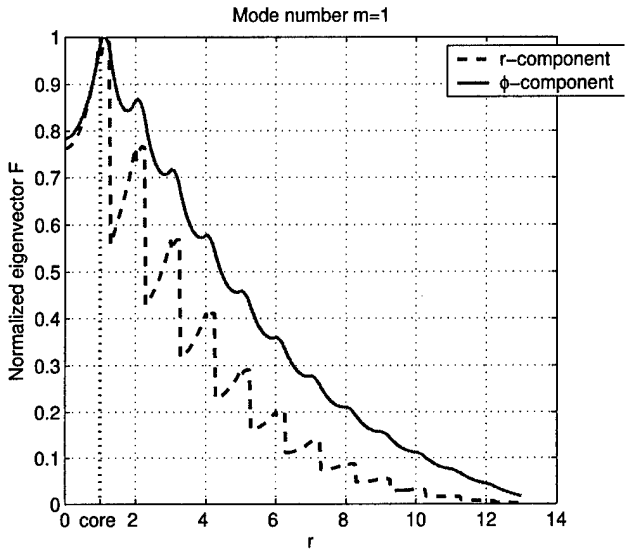

Figure 4: Field distribution with $m = 1$ and $\gamma = 1.03184$.

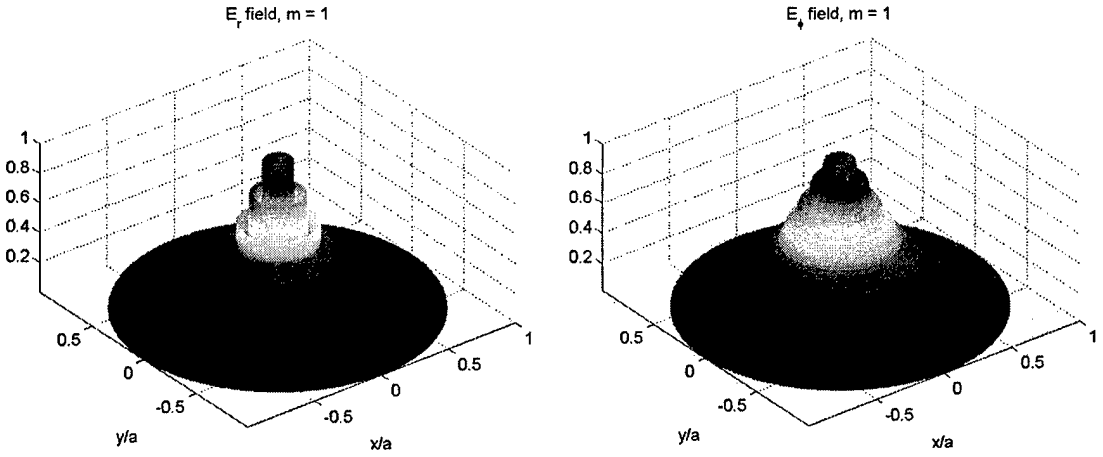

Figure 5: Intensity distributions with $m = 1$ and $\gamma = 1.03184$.

the air core and its neighboring layers. This suggests that low power-loss is possible for these fibers. In the microwave region, these fibers have radii between 7 mm and 19 mm. Furthermore, by comparing the corresponding solutions *gamma* ($m = 1$) in each case, for example, Figures6 and **??**, 8 and 22, 12 and 26 fibers with different layer thickness can confine wave in their air core more efficiently than those with same layer thickness.

4.3.1 Different layer thickness

Consider fibers with 6, 12, and 18 layers of dielectric pairs, that is, $n_{\text{air}}^{\text{core}}(n_H n_L)_k n_{\text{air}}^{\text{ext}}$ where $k = 6, 12, 18$. Fiber parameters are

$$n_{\text{air}} = 1,\ n_H = 4.6,\ n_L = 1.5,$$
$$d_{\text{core}} = 1,\ d_H = 0.25,\ d_L = 0.75.$$

In Table 4, solutions γ to (7) for $m = 1$ are listed for quarter-wavelength multilayered fibers whose high-index and low-index thicknesses are different.

Number of layers	γ
6 layers $\lambda = 4[d_{\text{core}} + 6(d_H + d_L)] = 28$	0.54353618
12 layers $\lambda = 4[d_{\text{core}} + 12(d_H + d_L)] = 52$	0.03063851 0.29596912
18 layers $\lambda = 4[d_{\text{core}} + 18(d_H + d_L)] = 76$	0.03105617 0.20275634

Table 4: Solutions γ for multilayered quarter-wavelength fibers with different number of layers. High-index and low-index thicknesses are different.

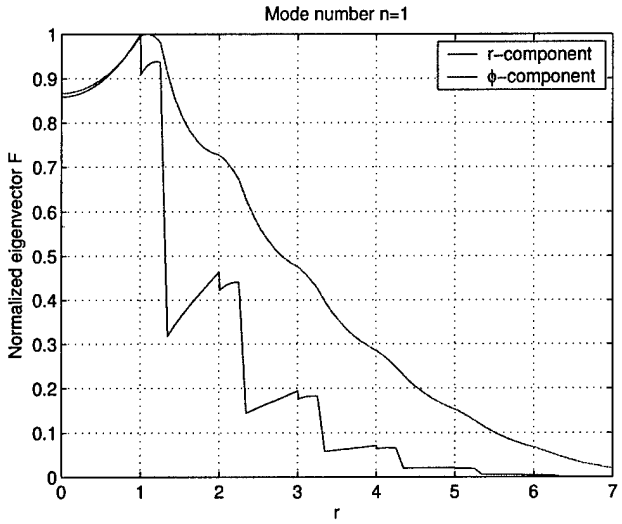

Figure 6: Normalized intensity profile in the 6-layer fiber of radius 7 mm with different refractive-index thicknesses: $\gamma = 0.54353618$.

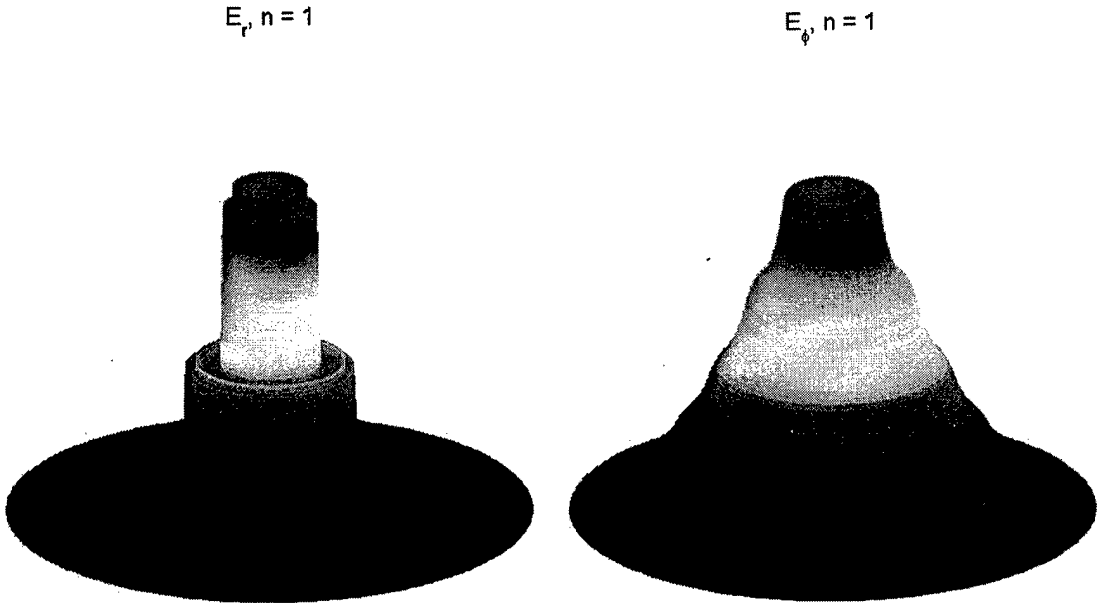

Figure 7: Normalized intensity distribution in the 6-layer fiber of radius 7 mm with different refractive-index thicknesses: $\gamma = 0.54353618$

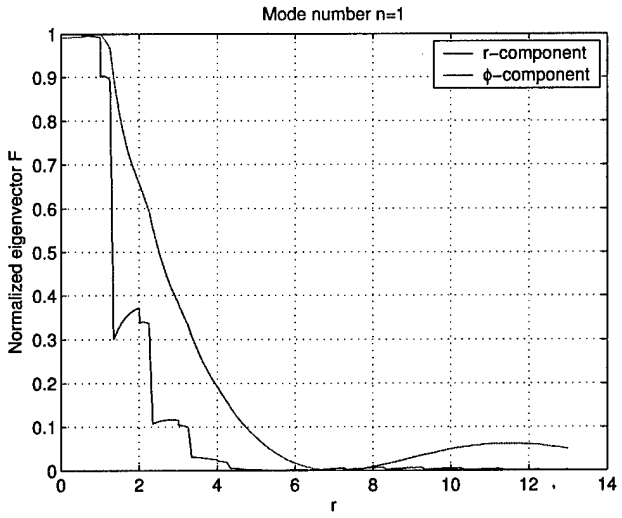

Figure 8: Normalized intensity profile in the 12-layer fiber of radius 13 mm with different refractive-index thicknesses: $\gamma = 0.03063851$

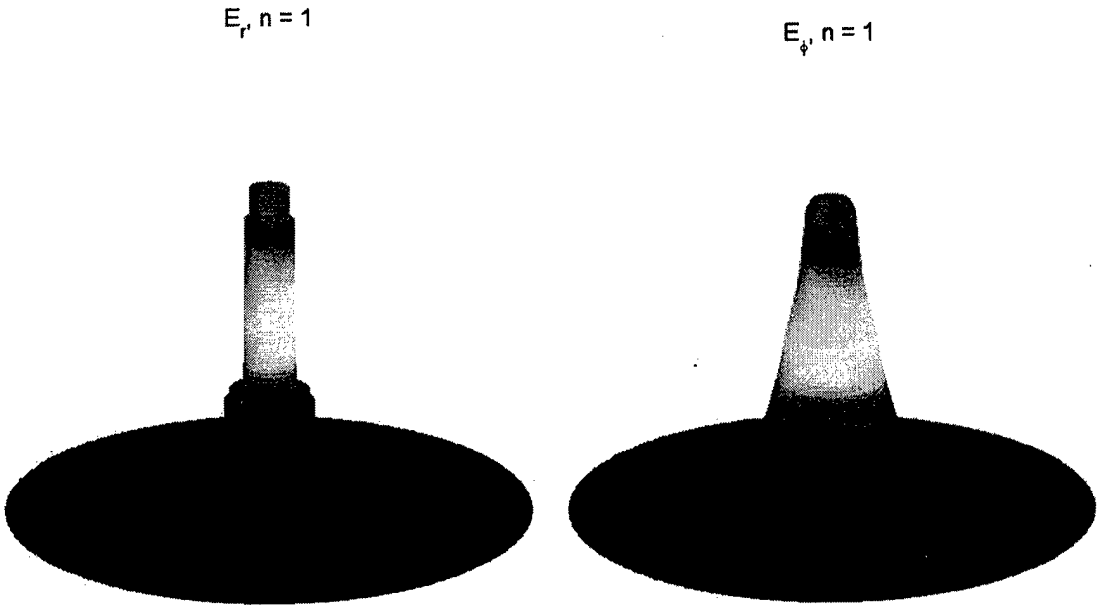

Figure 9: Normalized intensity distribution in the 12-layer fiber of radius 13 mm with different refractive-index thicknesses: $\gamma = 0.03063851$

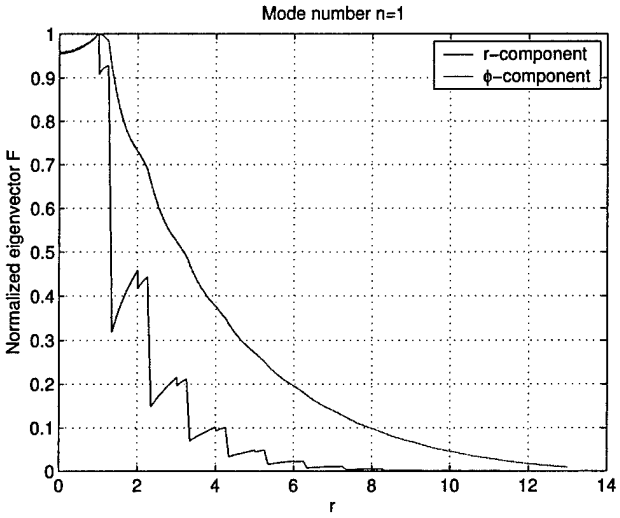

Figure 10: Normalized intensity profile in the 12-layer fiber of radius 13 mm with different refractive-index thicknesses: $\gamma = 0.29596912$

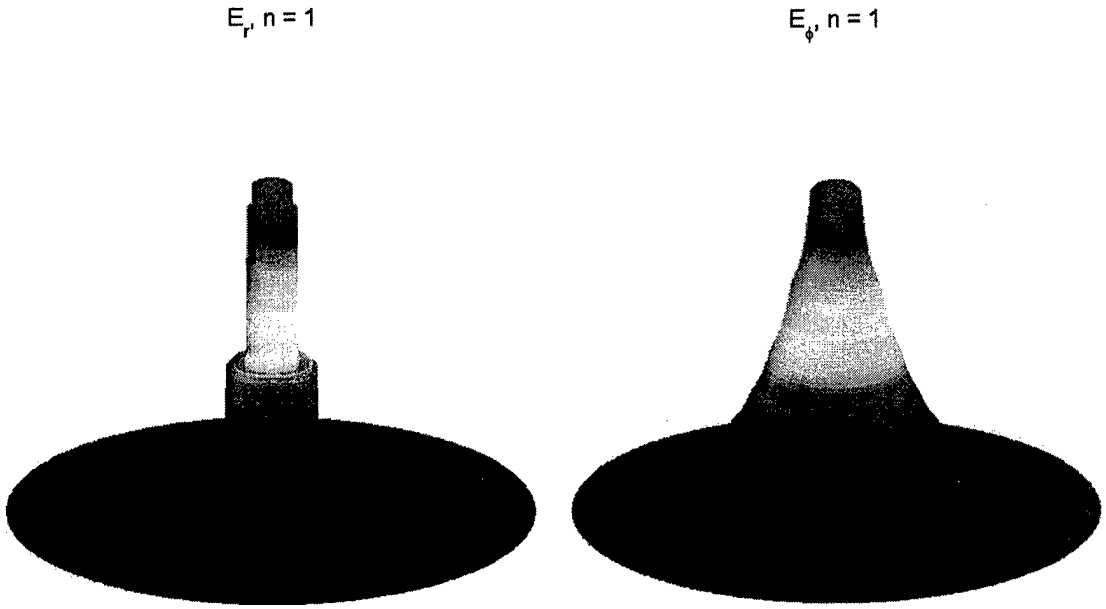

Figure 11: Normalized intensity distribution in the 12-layer fiber of radius 13 mm with different refractive-index thicknesses: $\gamma = 0.29596912$

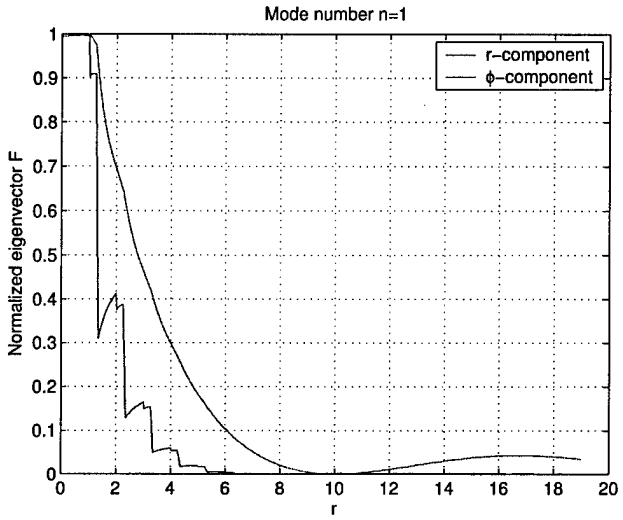

Figure 12: Normalized intensity profile in the 18-layer fiber of radius 19 mm with different refractive-index thicknesses: $\gamma = 0.031056172$

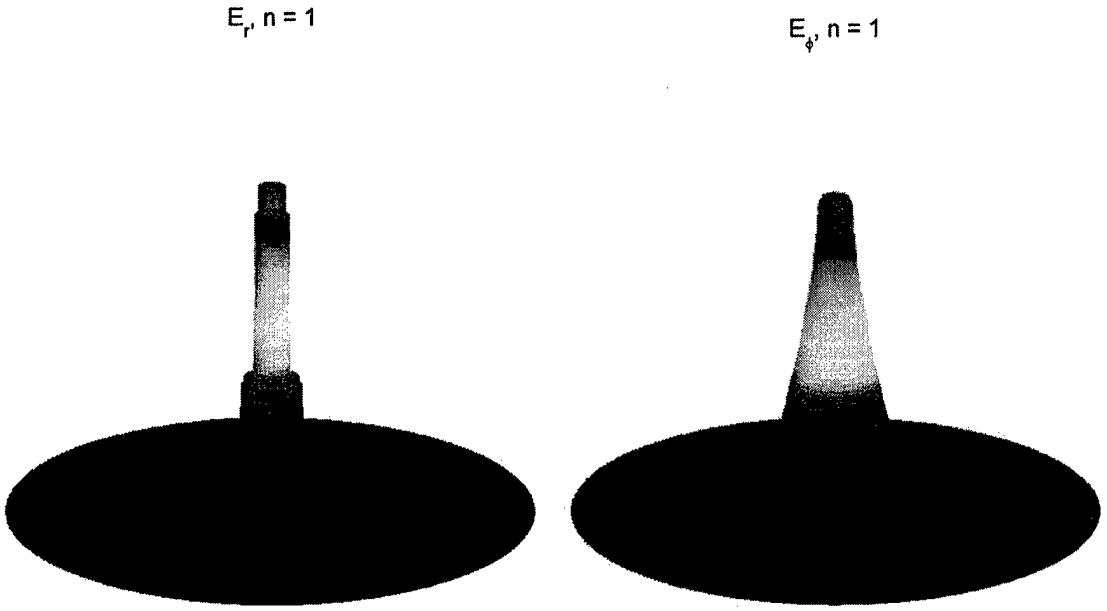

Figure 13: Normalized intensity distribution in the 18-layer fiber of radius 19 mm with different refractive-index thicknesses: $\gamma = 0.03105617$

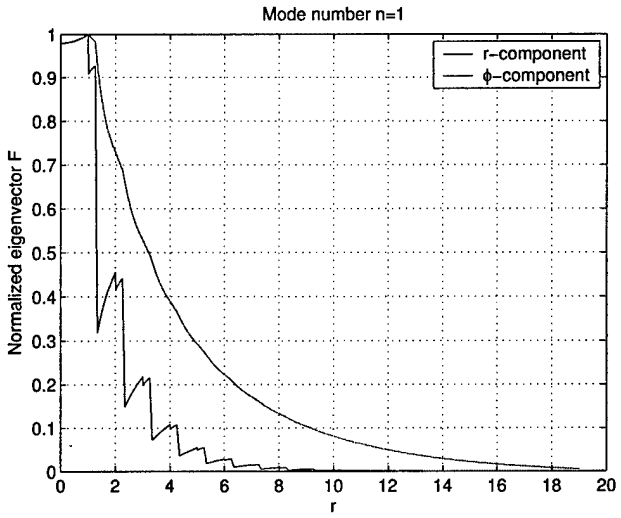

Figure 14: Normalized intensity profile in the 18-layer fiber of radius 19 mm with different refractive-index thicknesses: $\gamma = 0.20275634$

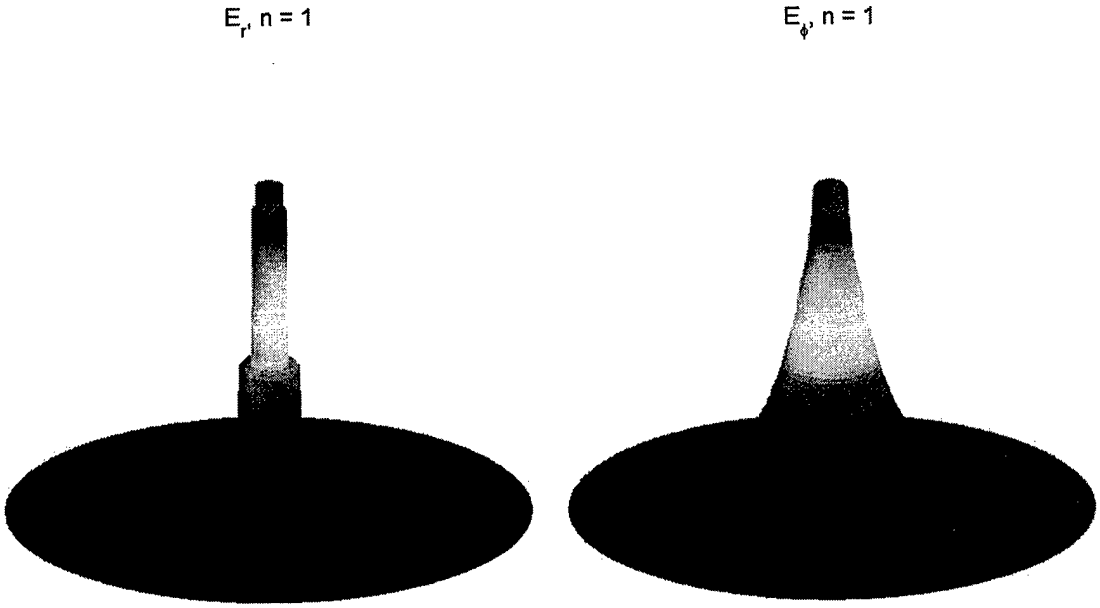

Figure 15: Normalized intensity distribution in the 18-layer fiber of radius 19 mm with different refractive-index thicknesses: $\gamma = 0.20275634$

4.3.2 Same layer thickness

Consider fibers with 6, 12, and 18 layers of dielectric pairs, that is, $n_{\text{air}}^{\text{core}}(n_H n_L)_k n_{\text{air}}^{\text{ext}}$ where $k = 6, 12, 18$. We assume that the high-index and low-index layers have the same thickness. Fiber parameters are

$$n_{\text{air}} = 1,\ n_H = 4.6,\ n_L = 1.5,$$
$$d_{\text{core}} = 1,\ d_H = 0.5,\ d_L = 0.5.$$

Solutions γ with $m = 1$ for different fibers are listed in Table 5.

Number of layers	γ
6 layers	0.26877105
$\lambda = 4[d_{\text{core}} + 6(d_H + d_L)] = 28$	0.34457807
	0.71278887
12 layers	0.21106533
$\lambda = 4[d_{\text{core}} + 12(d_H + d_L)] = 52$	0.38696444
18 layers	0.14845343
$\lambda = 4[d_{\text{core}} + 18(d_H + d_L)] = 76$	0.26511726

Table 5: Solutions γ for multilayered quarter-wavelength fibers with different number of layers. High-index and low-index thicknesses are equal.

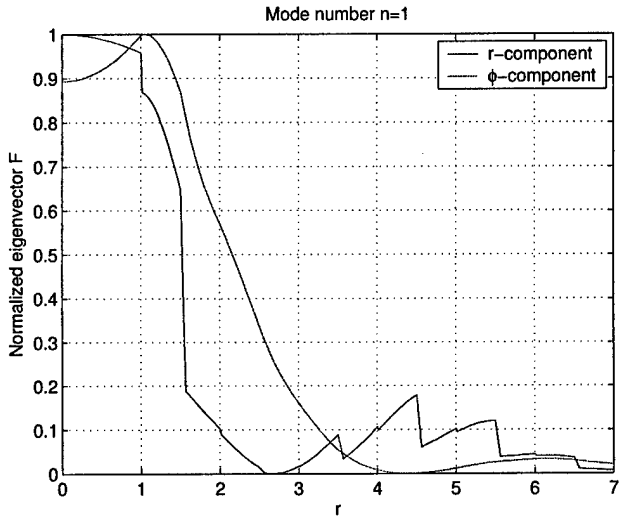

Figure 16: Normalized intensity profile in the 6-layer fiber of radius 7 mm with same refractive-index thicknesses: $\gamma = 0.26877105$

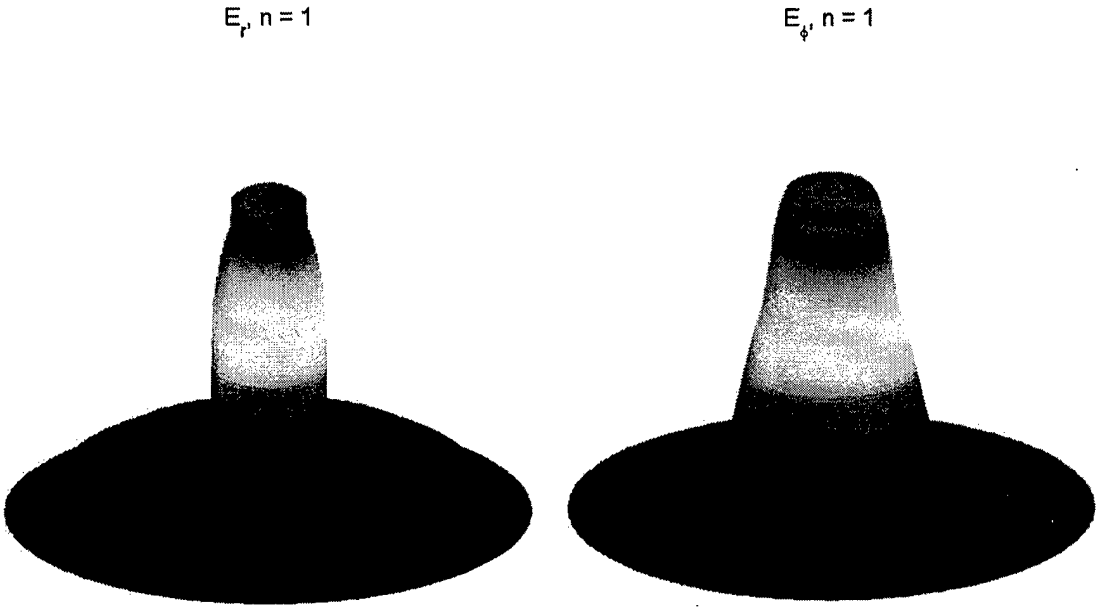

Figure 17: Normalized intensity distribution in the 6-layer fiber of radius 7 mm with same refractive-index thicknesses: $\gamma = 0.26877105$

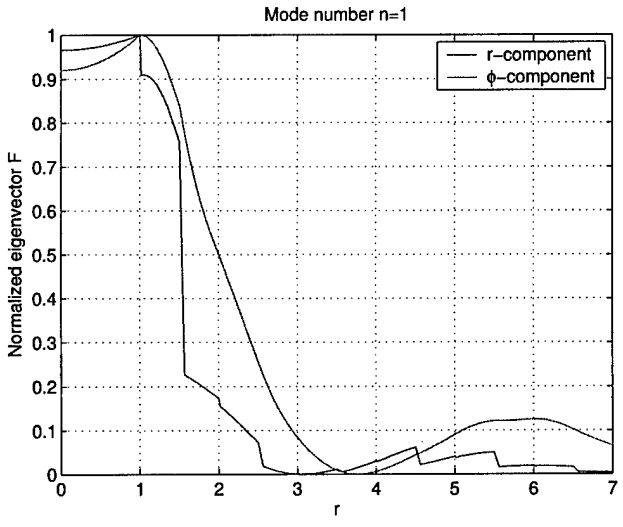

Figure 18: Normalized intensity profile in the 6-layer fiber of radius 7 mm with same refractive-index thicknesses: $\gamma = 0.34457807$

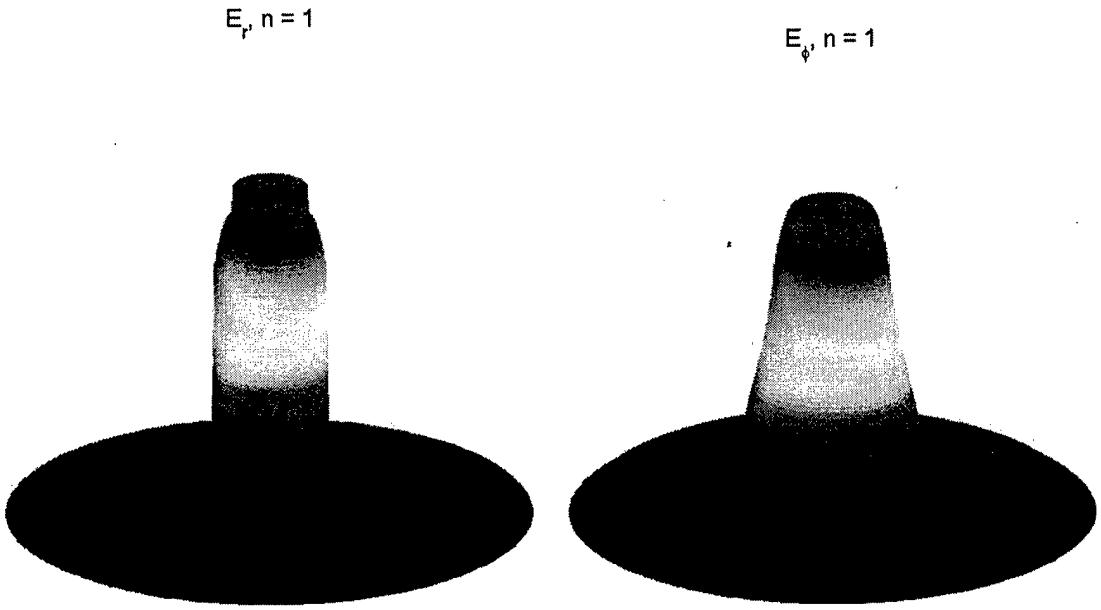

Figure 19: Normalized intensity distribution in the 6-layer fiber of radius 7 mm with same refractive-index thicknesses: $\gamma = 0.34457807$

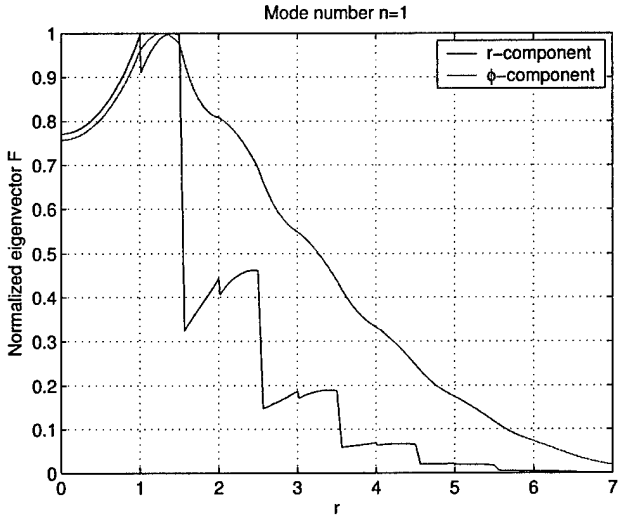

Figure 20: Normalized intensity profile in the 6-layer fiber of radius 7 mm: $\gamma = 0.71278887$

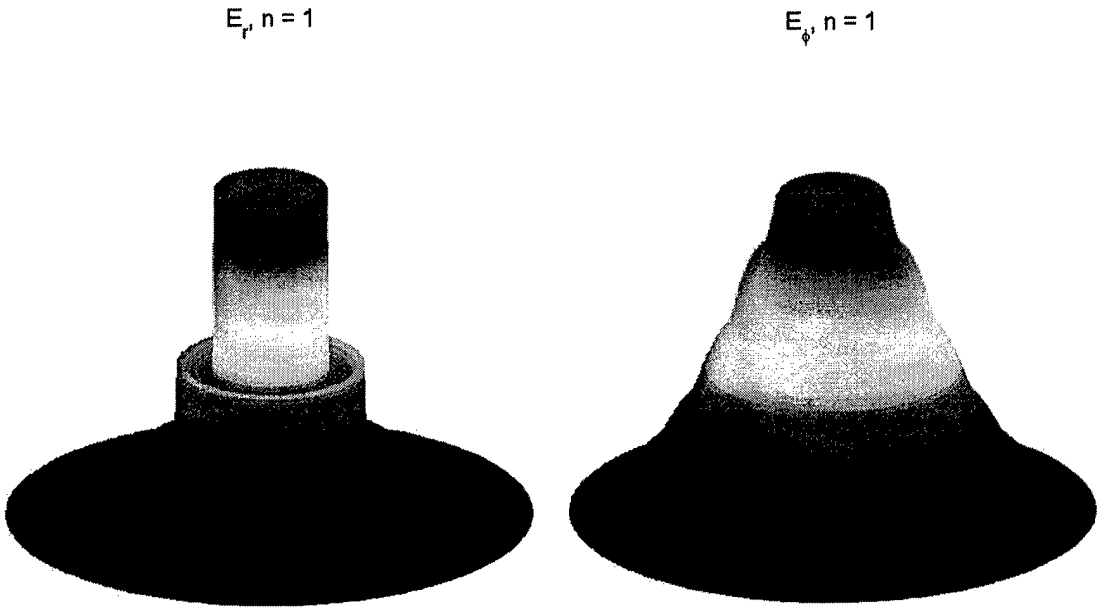

Figure 21: Normalized intensity distribution in the 6-layer fiber of radius 7 mm with same refractive-index thicknesses: $\gamma = 0.71278887$

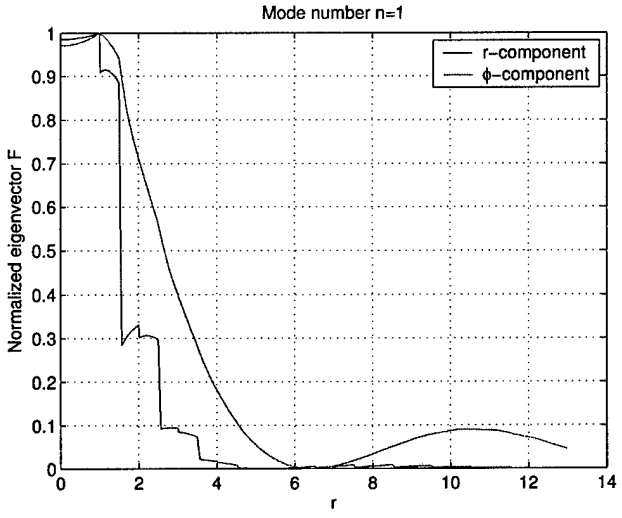

Figure 22: Normalized intensity profile in the 12-layer fiber of radius 13 mm: $\gamma = 0.21106533$

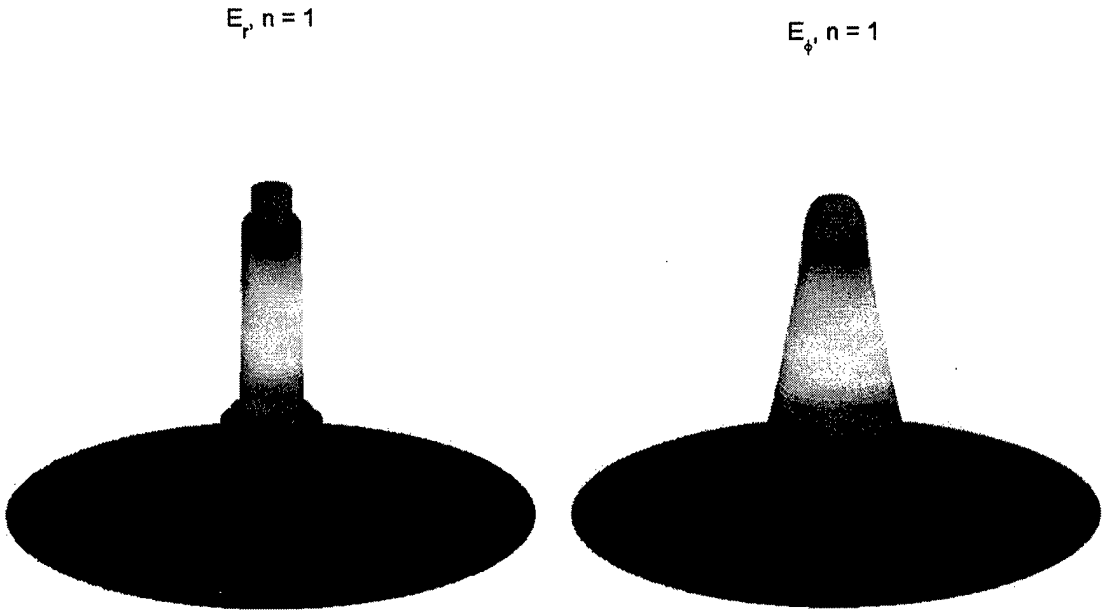

Figure 23: Normalized intensity distribution in the 12-layer fiber of radius 13 mm with same refractive-index thicknesses: $\gamma = 0.21106533$

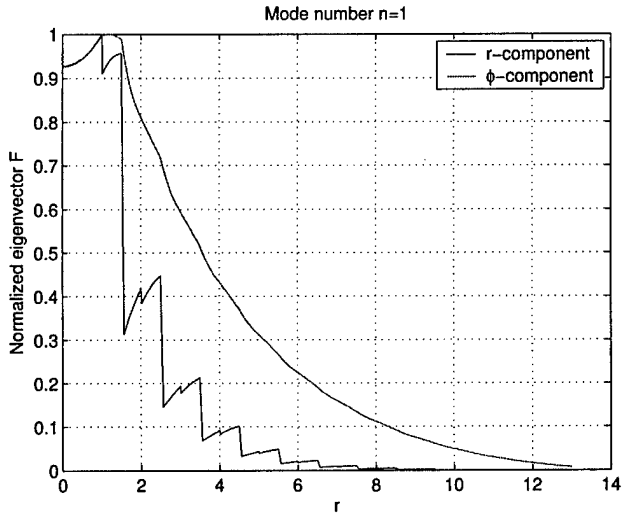

Figure 24: Normalized intensity profile in the 12-layer fiber of radius 13 mm with same refractive-index thicknesses: $\gamma = 0.38696444$

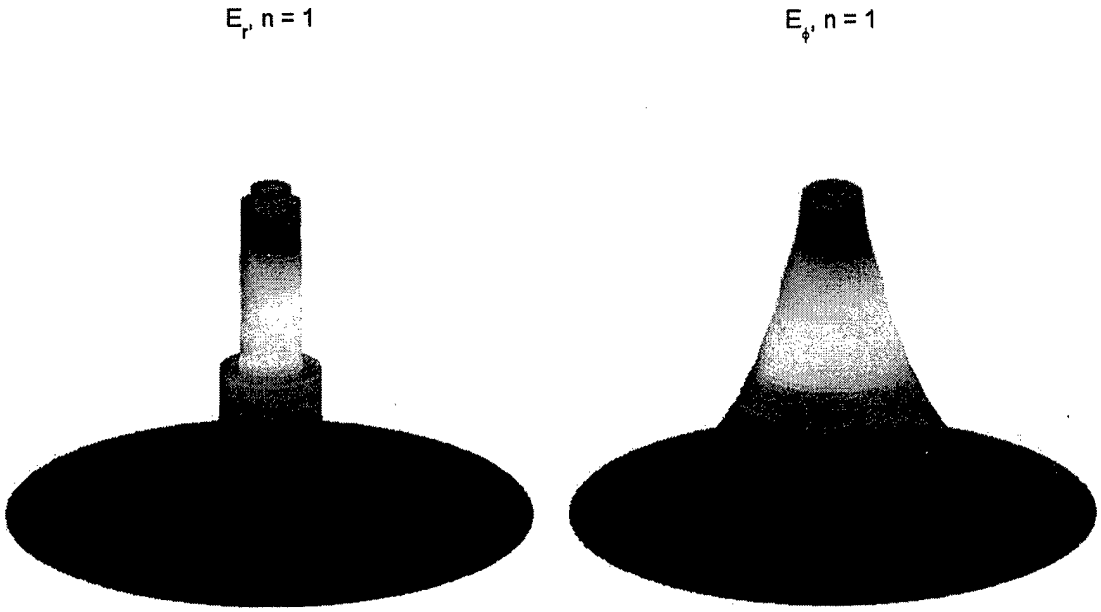

Figure 25: Normalized intensity distribution in the 12-layer fiber of radius 13 mm with same refractive-index thicknesses: $\gamma = 0.38696444$

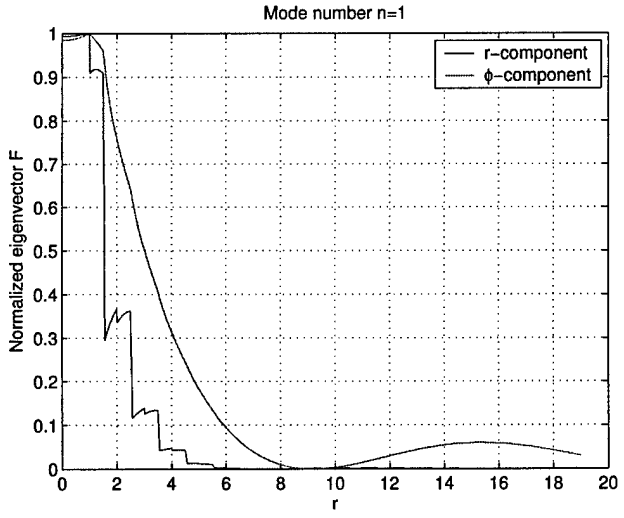

Figure 26: Normalized intensity profile in the 18-layer fiber of radius 19 mm with same refractive-index thicknesses: $\gamma = 0.14845343$

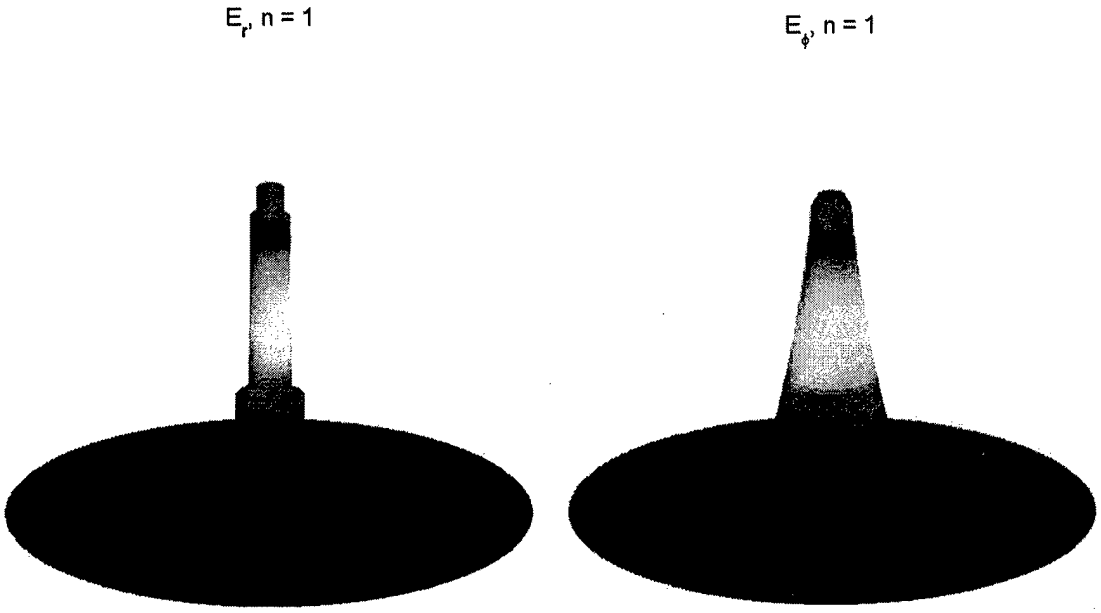

Figure 27: Normalized intensity distribution in the 18-layer fiber of radius 19 mm with same refractive-index thicknesses: $\gamma = 0.14845343$

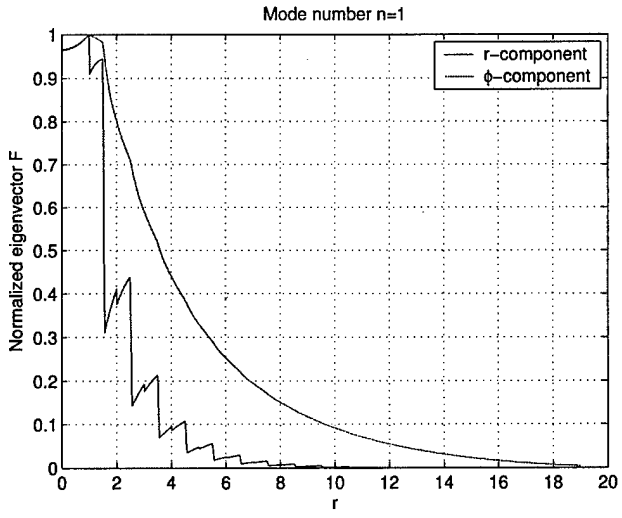

Figure 28: Normalized intensity profile in the 18-layer fiber of radius 19 mm with same refractive-index thicknesses: $\gamma = 0.26511726$

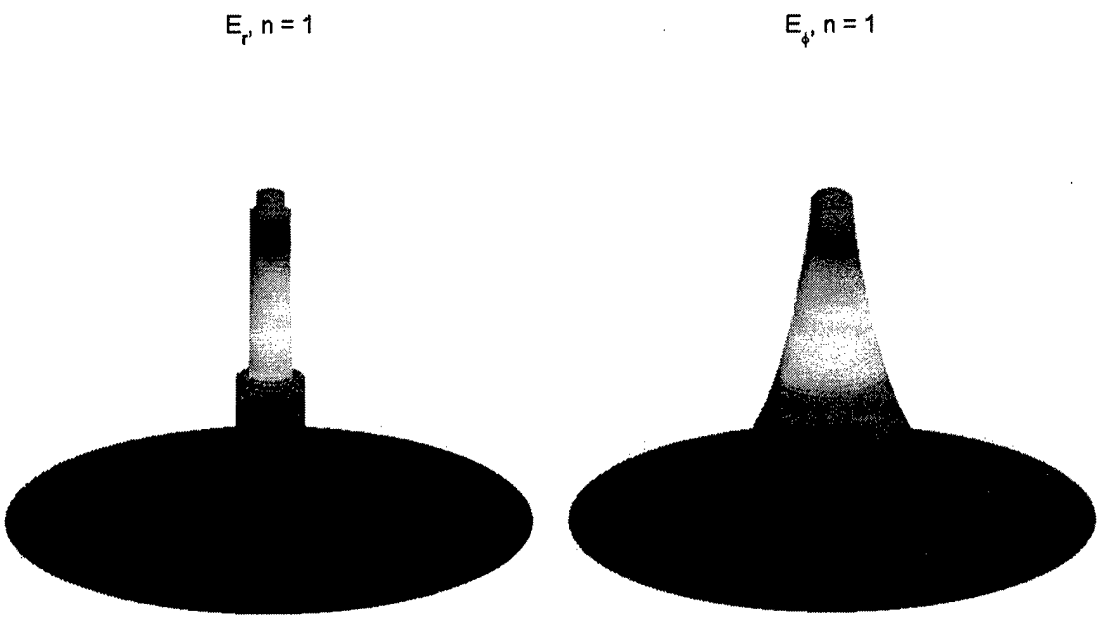

Figure 29: Normalized intensity distribution in the 18-layer fiber of radius 19 mm with same refractive-index thicknesses: $\gamma = 0.26511726$

5 Summary and plans

In this final report, we have summarized the progress made during the period September 1, 2002–September 30, 2003. We derive the integral equations for electric fields propagating in a fiber of arbitrary cross section and arbitrary refractive index.

Mathematical analysis of conventional optical fibers is rich and widely available in literature, for example [3, 9, 11] and references therein. It helps the advancement of optical fiber industry in understanding and designing fibers for data transport and telecommunications. In contrary, to our best knowledge, there is little of rigorous mathematical study of Bragg fibers due to the fabrication difficulty. Recently, the publications of *A dielectric omnidirectional reflector* [4], *An all-dielectric coaxial waveguide* [8], and *External reflection from omnidirectional dielectric mirror fibers* [7] in *Science* report successful fabrications of omnidirectional reflectors and multilayered fibers for *optical wavelengths*. These articles create a new interest in studying low-loss Bragg fibers at microwave and millimeter wavelengths for radar applications. From previous examples in Section 4, multilayered fibers of radii between 7 mm and 19 mm concentrate wave propagation within their air core for wavelengths in the microwave range. Hence, they can be very useful in radar technology.

A thorough analysis of the integral operators described in Section 2 is needed. Their spectral properties can be studied with functional analysis. A priori knowledge of the band structure of the integral operators will be very important in designing accurate and fast numerical algorithms. Possible problems such as the existence of spurious modes can also be addressed and remedied if one can predict the number and location of propagating modes. Error and convergence analysis of the presented numerical method needs to be done rigorously. This study is very important,

especially when the method is applied in optimal designs. We plan to perform these analyses rigorously.

For radar applications, propagating power of a fiber is probably the most important property that has great impact on the fiber usefulness. Hence, optimizing its power over parameters such as number of layers, layer thickness, and refractive index, is of great interest. We plan to determine an appropriate objective function to be optimized by an accurate and fast optimizing algorithm which can be parallelized for different computer platforms.

Acknowledgement

The first author would like to thank Dr. William Kent and Dr. Gregory Wilson at Mission Research Corporation in Dayton for helpful discussions and comments. Dr. Kent brought to my attention the valuable applications of low loss fibers in the radar world.

References

[1] F. Abeles, *Investigations on the propagation of sinusoidal electromagnetic waves in stratified media. Application to thin films*, Ann. Phys. **5** (1950), 596–.

[2] ———, *Investigations on the propagation of sinusoidal electromagnetic waves in stratified media. Application to thin films. II. Thin films*, Ann. Phys. **5** (1950), 706–.

[3] A. Bamberger and A.S. Bonnet, *Mathematical analysis of the guided modes of an optical fiber*, SIAM J. Math. Analys. **21** (1990), no. 6, 1487–1510.

[4] Yoel Fink, Joshua Winn, Shanhui Fan, Chiping Chen, Jurgen Michel, John Joannopoulos, and Edwin Thomas, *A dielectric omnidirectional reflector*, Science **282** (1998), 1679–1682.

[5] Sh.A. Furman and A.V. Tikhonravov, *Basics of Optics of Multilayer Systems*, Basics of, Editions Frontieres, Singapore, 1992.

[6] Gene H. Golub and Charles F. Van Loan, *Matrix Computations*, third ed., Johns Hopkins University Press, Baltimore, 1996.

[7] S.D. Hart, G.R. Maskaly, B. Temelkuran, P.H. Prideaus, J.D. Joannopoulos, and Y. Fink, *External reflection from omnidirectional dielectric mirror fibers*, Science **296** (2002), 510–513.

[8] M. Ibanescu, Y. Fink, E.L. Thomas, and J.D. Joannopoulos, *An all-dielectric coaxial waveguide*, Science **289** (2000), 415–419.

[9] P. Joly and C. Poirier, *A numerical method for the computation of electromagnetic modes in optical fibers*, Math. Meth. in Appl. Sciences **22** (1999), 389–447.

[10] Rainer Kress, *Linear Integral Equations*, second ed., Springer-Verlag, New York, 1999.

[11] Rolando Magnanini and Fadil Santosa, *Wave propagation in a 2-D optical waveguide*, SIAM J. Appl. Math. **61** (2000), no. 4, 1237–1252.

[12] G. Ouyang, Y. Xu, and A. Yariv, *Theoretical study on dispersion compensation in air-core Bragg fibers*, Optics Express **10** (2002), no. 17, 899–908.

[13] Y. Xu, G. Ouyang, R. Lee, and A. Yariv, *Asymptotic matrix theory of Bragg fibers*, J. Lightwave Tech. **20** (2002), no. 3, 428–440.

[14] A. Yariv and P. Yeh, *Optical Waves in Crystals. Propagation and Control of Laser Radiation*, John Wiley & Sons, New York, 1984.

[15] P. Yeh, A. Yariv, and E. Marom, *Theory of Bragg fiber*, J. Opt. Soc. Am. **68** (1978), 1196–1201.